2

Remote Sensing for Mapping and Monitoring Wetlands and Small Lakes in Southeast Brazil

Philippe Maillard[1], Marco Otávio Pivari[2] and Carlos Henrique Pires Luis[1]
[1]*Universidade Federal de Minas Gerais*
[2]*Instituto Inhotim*
Brazil

1. Introduction

Wetlands and small lakes are areas with great ecological value that are increasingly threatened through excessive pressure on water resources. In some cases, this pressure can lower the aquifer and result in a significant reduction of the area of small lakes or the drying out of wetlands. In other cases, logging, road building and other degradations of the surroundings of lakes can increase nutrients loads that reach the water and alter the state of these lakes towards eutrophication and reduction of the open water surface through colonization by aquatic plants. The first requirement to help protect these areas is a thorough mapping and monitoring of the changes that affects them: past, present and future. Many of these areas are poorly known and have not been mapped thoroughly and most have never been monitored. Remote sensing is the only effective means to perform both tasks by enabling rapid mapping of their situation both past and present. While images from the recent generations of Earth observing satellite and sensors come in a wide range of spatial resolution up to about half a meter, historical data at medium-scale resolution can provide a record of past situations and help determine an evolutionary trend.

This chapter is dedicated to the description of methods for the cartography of small lakes using high-resolution data for actual or near-actual mapping and medium-resolution historical data for determining the evolutionary path of these areas in the last three decades. In particular, the accent is given to two distinct approaches: 1) the use of region-based unsupervised segmentation and classification to delineate small lakes, and 2) multi-temporal image analysis of long sequences of images to assess changes of both small lakes and wetlands communities. Two case studies are described to illustrate these methods.

2. First case study: The Rio Doce lake system

It as been observed in the Brazilian Pantanal, that the process of aquatic plant succession starts with the emergence of free floating macrophytes followed by colonization of epiphytes. The latter can be subtituted by paludian plant of higher stature. Eventually, if this process is pursued without interruption, it can culminate by the emergence of floating island and the constitution of an organic soil (Pivari et al., 2008; Pott & Pott, 2003). Pantanal wetlands are subject to alternate flooding and drought that cause these floating islands to drift with the current and wind or to dry out causing the death of its vegetation (Junk & Silva, 1999). Conversely, in the "Rio Doce" lake system of the present study (Figure 1), the water level is

almost constant throughout the year (average variation of less than 1 m), therefore the floating islands that form tend to perpetuate and grow and can eventually occupy the whole area of the lake.

Fig. 1. Location of the Rio Doce study area including the Rio Doce State Park (black thick line).

Although the process of floating island formation is a natural one, in certain cases it can be initiated or accelerated by human interference. Our hypothesis is that a significant degradation of the surroundings of the lakes can cause an increase in sediments and nutrients load that can alter the state of the lake from oligotrophic to eutrophic. This new chemical balance is known to be beneficial for the development of free floating macrophytes species. If the aquatic environment is lentic, isolated and perennial (without seasonal flooding pulses) the emergence of macrophyte tend to colonize an ever increasing area of the lake and will eventually lead to the formation of floating islands. These floating island can, in turn grow indefinitely until the whole lake is covered. There are a number of these completely covered lakes in the Rio Doce lake system. Although we speculated that it is the degree of human interference (logging, agriculture, fertilizers, road construction, etc.) that is the main factor responsible for causing some lakes to be colonized by floating islands and others not, a clear trend could not be verified. Some lakes appear to have seen their open water area increased despite the degradation of their surroundings.

The objective of this study is to verify if the history of recent human interferences can help explain the formation of large areas of floating islands within the Rio Doce lake system. To do so, we have used a 20 years temporal series of Landsat images to assess the behavior of these lakes in terms of their area of open water and determine if it can be associated with the degree of human interference. A high resolution Ikonos[1] mosaic of images and a RapidEye[2] mosaic were also used to complement our field data for the initial delineation of the lakes.

2.1 Material and method

2.1.1 Study area

The Rio Doce valley is located in the eastern part of the state of Minas Gerais and is an important physiographic feature of Southeastern Brazil. The relief is strongly ondulating at an average altitude of about 250 m a.s.l. and varies between 195 and 525 m a.s.l. with many depressions occupied by lakes (Gilhuis, 1986). Annual rainfall ranges between 1000 and 1250 mm and the climate by is hot and humid (Köppen: Aw) megathermic, with a distinct dry (April-September) and rainy season (October to March).

The Rio Doce lake district is the third largest lake system in the Brazilian territory (Tundisi et al., 1981). According to Esteves (1988), these water bodies originated in the Pleistocene through a blocking of the mouth of former tributaries of the Doce and Piracicaba rivers under the influence of an epirogenetic shift. This also explains the continuity and depth (up to about 30 m) of the lakes, meandering their ways.

The Rio Doce lake system is situated in the Atlantic Forest domain (*Mata Atlântica*), where the vegetation is classified as mesophilous semi-deciduous forest (Veloso et al., 1991). The dense native forest that naturally surrounds the lakes prevents the entry of large quantities of allochthonous material (sediments), allowing the limnological characteristics of these water bodies to sustain over time without large fluctuations in their physicochemical characteristics and in the chemical composition of their sediments (Meis(de) & Tundisi, 1986). Under these conditions, the lakes generally present an oligotrophic state and a low diversity of dominant macrophytes (Ikusuma & Gentil, 1985).

However, these lakes are in various states of health and those within the boundaries of Rio Doce State Park (RDSP) are generally well preserved. In 2009 some of the lakes located in this protected area have been recognized internationally as a Ramsar Site (site 1900 http://www.ramsar.org/), with an important wetland area for the conservation of biodiversity as well as economic, cultural, scientific and recreational resources (SMASP 1997). Most of the lakes located outside the RDSP boundaries have had their surrounding native vegetation devastated, a factor that changed their original oligotrophic status to eutrophic. Since the 1950s these areas have suffered from various human activities, beginning with the removal of vegetation for charcoal production to supply metallurgical plants. Today, these areas are used for extensive plantations of eucalyptus and are intertwined by an extensive network of paved and unpaved roads. Other sources of threat include residential and industrial pollution, hunting and predatory fishing, fragmentation of remaining habitat and introduction of exotic species.

[1] An American commercial satellite operated by Space Imaging Corporation and producing panchromatic and multispectral images with ground resolutions of one and four meters respectively.
[2] A German-owned constellation of five satellites producing five meter resolution multispectral imagery.

2.1.2 Satellite and cartographic data

The imagery data available for this project came in the form of an Ikonos mosaic of 2006, a RapidEye set of images of 2010, Landsat historical data and out-of-date cartographic data (last updated in the 70's). The Ikonos mosaic was already pan-sharpened [3] and was made available by the Forest Institute of Minas Gerais (*Instituto Estadual de Florestas - Minas Gerais*). The RapidEye images with a ground resolution of 5 m were also made available by the IEF and were used to complete the Ikonos mosaic to the North, South and East. The Landsat database was constituted of 17 Landsat-5 TM images covering the 1989-2010 period, two of which had to be excluded because of their poor quality (Table 1). The cartographic data consisted mainly of the hydrographic network which was added to map products.

Date	Quality	Date	Quality	Date	Quality
04/07/1985	good	05/07/1997	* rejected	24/07/2004	good
04/05/1986	good	08/07/1998	good	14/05/2007	good
15/07/1989	good	28/08/1999	good	05/09/2008	good
27/08/1993	good	27/06/2000	good	07/08/2009	good
01/10/1994	good	27/04/2001	good	26/08/2010	good
18/07/1996	good	20/06/2003	* rejected		

Legend: *images with too many clouds or haze

Table 1. List of Landsat-5 TM images (orbit/scene 217-73 and 74) used in this study along with a quality assessment.

Field work was conducted over a period of four years in which as many as 20 lakes were visited and over 200 species of aquatic plants were collected and identified (Pivari et al., 2008). Positional data was also acquired using a navigation GPS to register the images to a common cartographic projection (UTM 23 South).

Because no survey of the lakes was done, our approach was to use the Ikonos and RapidEye images as basis for the contouring of all the lakes while accounting for possible positioning inaccuracies by applying a buffer of 75 meters outside the interpreted vectors. These vector would subsequently be used to eliminate undesirable classified pixels and areas. At the same time, based on the knowledge acquired in the field, the wetland areas were divided into four different classes: 1) macrophytes with visible open water, 2) bogs, 3) peatland, and 4) floating islands. Figure 2 shows examples of these wetland classes.

Our main goal being to determine if the formation of floating islands can be related to the degradation of the surroundings, these wetland classes were considered as a whole and it was assumed that what was not classified as open water belonged to the wetland class, that is within the vicinities of the lakes. The main reason for not considering these different types of wetlands was that they were not spectrally separable from the tests we conducted. We also had insufficient validation data to do a full scale classification of aquatic communities.

2.1.3 Lake classification with MAGIC

To classify the open water areas of the lakes, a region-based unsupervised classification approach was adopted where two classes were sought: water and non-water. The MAGIC

[3] Pan-sharpening involves resampling the 4 m multispectral imagery to 1 m using the panchromatic channel.

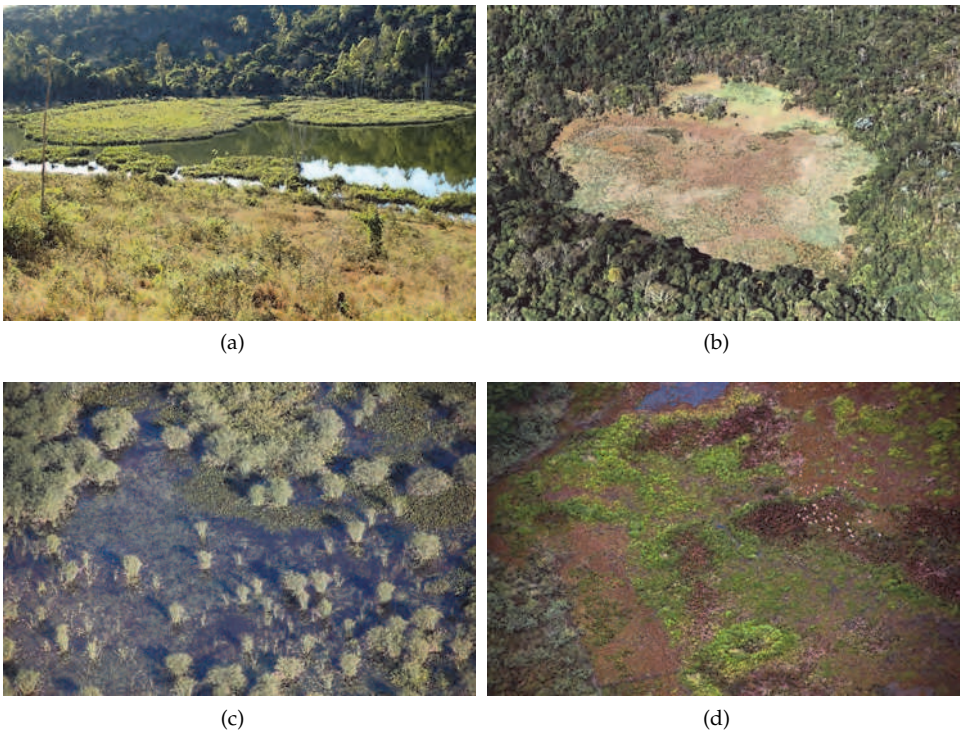

Fig. 2. The four main types of wetland encountered in the study region: (a) floating island, (b) peatland, (c) macrophytes with open water and (d) bogs.

(©2010 Systems Design Engineering, University of Waterloo, Canada) program (Clausi et al., 2010) is the product of an ongoing research (actually in version 2) and was chosen to segment and classify the images for having yielded excellent results in several other studies (Barbosa & Maillard, 2010; Maillard et al., 2008). MAGIC is an acronym that stands for "MAp Guided Ice Classification" because it was originally developed as a tool for classification of sea ice types. With new applications being tested and implemented, the "I" in MAGIC might eventually stand for "image".

The classification of MAGIC is unique in its implementation and the principles it embodies. It is an hybrid segmentation-classification approach that uses two different paradigms: "watershed" and Markov Random Fields (MRF). The segmentation is started by applying a "watershed" algorithm that produces a preliminary segmentation and generates segments (areas) of 10-30 pixels depending on the noise level in the image. The "watershed" algorithm implemented in MAGIC was developed by Vincent & Soille (1991) and divides an image into segments with closed boundaries. The "watershed" algorithm first looks for local minima and then works by region growing until it finds a divide line with another "catchment" area. However, it tends to oversegment the image, a characteristic that MAGIC takes advantage of in order not to "miss" any object.

Conversely, the MRF model (Li, 1995) assumes that the conditional probability of a pixel given its neighbors is equal to the conditional probability of that pixel given the rest of the image. This makes it possible to consider every pixel within its neighborhood as an independent process (Tso & Mather, 2001) and to compute the conditional probability of a pixel belonging to a given class using the Bayes rule:

$$P(Y_i|x) = \frac{p(x|Y_i)P(Y_i)}{\sum_i [p(x|Y_i)P(Y_i)]} \tag{1}$$

where $p(x|Y_i)$ is the conditional distribution of vector x given class/segment Y_i and $P(Y_i)$ is the prior probability of the Y_i class. Suppose that the energy associated to the prior probability is E_r and that E_f represents the energy of the spatial context $p(x|Y_i)$, then the general energy formula is given by Geman et al. (1990):

$$E = E_r + \alpha E_f \tag{2}$$

where E_f is the energy form of feature vector f having k dimensions. Assuming a Gaussian distribution E_f can be modeled as:

$$E_f = \sum_{s,m=Y_s} \left\{ \sum_{k=1}^{K} \left[\frac{(f_s^k - \mu_m^k)^2}{2(\sigma_m^k)^2} + \log(\sqrt{2\pi}\sigma_m^k) \right] \right\} \tag{3}$$

where μ_m and σ_m are the mean and standard deviation of mth class in the kth feature vector. E_r represents the energy of the labels (classes) in the neighborhood of the pixel being analyzed based on a system of *clique* (generally pairs or triplets of contiguous pixels):

$$E_r = \sum_s \left[\beta \sum_{t \in N_s} \delta(y_s, y_t) \right] \tag{4}$$

where y_s and y_t are the respective class of pixels s and t (inside the *clique*), and $\delta(y_s, y_t) = -1$ if $y_s = y_t$ and $\delta(y_s, y_t) = 1$ if $y_s \neq y_t$. β is a constant. In the absence of training samples to determine the labels of the pixels of the *clique*, these are initially randomly determined and gradually stabilize by iteration.

In equation 2, α is a parameter that sets the proportions of the relative contribution of E_r and E_f within E. The adaptation of Deng & Clausi (2005) adopted in MAGIC makes α iteratively change the weighting between the spectral (global) and spatial (local) components; early iterations favor the spectral component and increased iterations gradually increase the weight on the spatial component.

MAGIC is unique in the sense that instead of working on pixels, it uses the actual segments produced by the "watershed" algorithm. These segments are arranged topologically, so that all contiguous segments can be determined through an adjacency graph or RAG (Region Adjacency Graph). MAGIC will then merge contiguous segments if the union produces a decrease in the total energy of the neighborhood defined above.

The advantage of the MRF model is its inherent ability to describe both the spatial context location (the local spatial interaction between neighboring segments) and the overall distribution in each segment (based on parameters of distribution of spectral values for example). This new approach was entitled "Iterative Region Growing Using Semantics" or

IRGS and is described in Yu & Clausi (2008). Because MAGIC associates the segments to a predefined set of classes, it is considered a region-based unsupervised classification system.

MAGIC incorporates a number of innovative features such as 1) importing vector polygons to guide or restrict the classification (hence the "map-guided"), 2) a number of other segmentation approaches both traditional (*e.g.* K-means, gaussian mixture) and MRF-based, 3) the ability to compute texture features (grey level co-occurrence matrix and gabor) and 4) a functional graphical user interface (GUI). Figure 3 illustrates the GUI of MAGIC with the classification results for the Landsat 2010 image and the pop-up window for the IRGS algorithm.

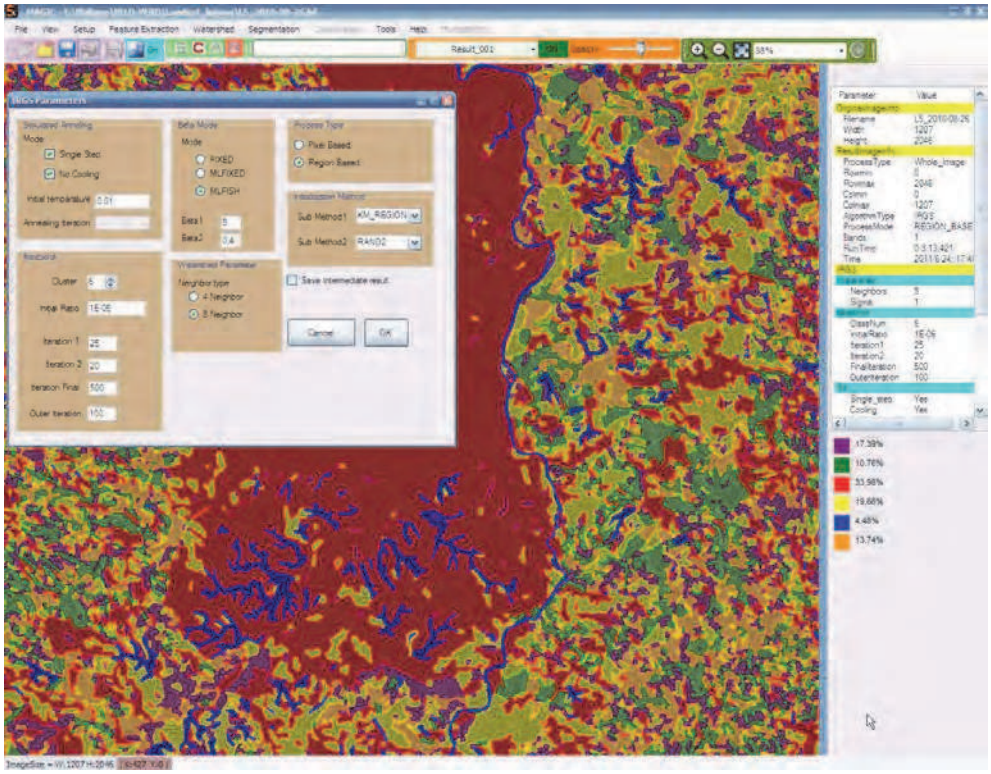

Fig. 3. The graphical user interface (GUI) of MAGIC also showing the pop-up window for the IRGS segmentation / classification.

The unsupervised classification was performed on all Landsat images using exclusively the mid-infrared band (band 5) generally considered the best option for separating land from water (Ji et al., 2009; Xu, 2006). This approach also included rivers in the classification results which were eliminated using the lake buffers. Other "misclassified" pixels (dark shadows, tiny reservoirs) were also eliminated by the process.

2.1.4 Area calculation and statistical modeling

The calculation of the open water area in each lake was a straight forward operation performed by simply counting the water pixels within each individual lake contour (plus buffer). Each lake was treated as an individual "area of interest" for witch a statistics calculation yielded the total number of non-zero pixels. The area of each lake and each year was organized into a worksheet and processed using MiniTab (Copyright ©2011 Minitab Inc.). Because many small lakes "disappeared" during the period analyzed, some of which could "reappear" some years after, their inclusion into the regression processed posed an analysis problem and so it was decided to retain only the lakes larger than 10 hectares. This was also partly due to the resolution of the Landsat images (0.9 ha) that did not allow a satisfactory precision for very small areas. Simple linear regression was performed between the area of all remaining lakes and the time represented by the year of the Landsat images. The slope parameter of the regressions (provided it was statistically significant) was used to determine the trend in the behavior of the open water areas of the lakes through the 1989 - 2009 period.

2.2 Results

2.2.1 Open water classification

Because MAGIC is unsupervised and the user only feeds in the number of classes (and a region weight parameter that controls the merging of neighboring segments), it is normally better to specify more classes than actually needed so that the clusters in the spectral domain are more restrictive and more consistent. In this case, after a few trials, we found that six classes worked best and could be adopted for all 15 images. The non-water classes are then eliminated by defining which class number represents water (which is not necessarily the same all the time since class numbers are attributed randomly). The next step consisted in eliminating lakes smaller than 10 ha, rivers and any pixel being wrongly attributed the same class as water like very dark shadows (very rarely). The vectorized lakes interpreted from the Ikonos and RapidEye images with a 75 m buffer was used as a mask to retain only the 147 lakes larger than 10 ha. Figure 4 illustrates this process.

Between lakes, peatbogs, and swamps, there were 765 interpreted "objects", more than half of which (399) did not have open water at any time, or did not pertain to the Rio Doce lake system leaving some 366 "objects" with open water. However, only 173 had open water in all 16 years analyzed. The graph in Figure 5 shows the number of lakes with open water for each year of the 16 Landsat images as well as the number of lakes considering the number of years without open water. From the subjective analysis of both curves, we estimate that there are usually between 240 and 260 lakes. We also found that this number appears to be slowly increasing with time, which might be the results of more restrictive land use and more protective measures from both the authorities and the forestry companies.

2.2.2 Regression: Open water area *vs* year

Despite the fact that an average of $\approx$ 250 lakes have open water, only 107 lakes were left after the elimination of the lakes that had more than four years without open water because of the negative effect it would have of the regression analysis. One hundred and seven (107) regressions were done using the area of the lake as dependent and the year as independent. Of these, only the regressions with a coefficient of determination above 0.5 were retained and only when a clear trend (growing or shrinking) could be identified ($\mid slope \mid > 0.003$). This left

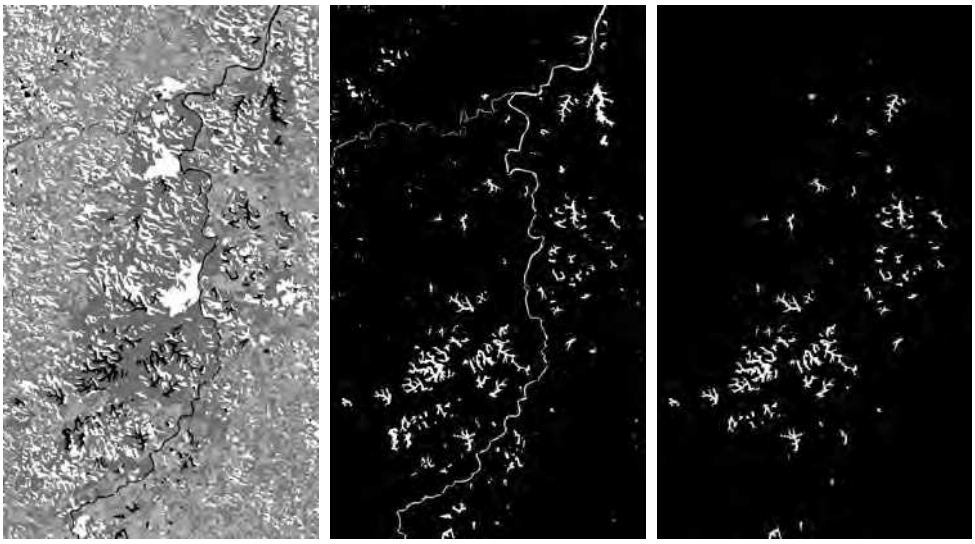

(a) (b) (c)

Fig. 4. Results of the open water classification for lakes larger than 10 ha and for the year 2009: a) the classification results of the unsupervised region-based classification using 6 classes, b) after elimination of the non-water classes, c) after eliminating small lakes and rivers.

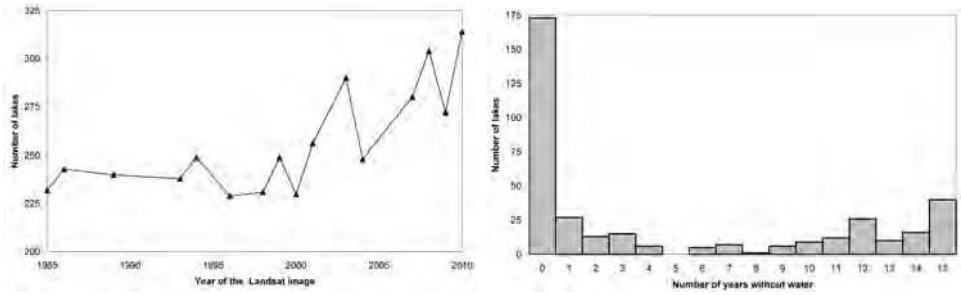

(a) (b)

Fig. 5. Graph showing in a) the number of lakes for each year studied and, in b) the number of lakes considering the number of years without open water (zero meaning that the lakes have open water in all years, 15 meaning that these lakes had no open water in 15 of the 16 years).

a total of 27 lakes for which the slope of the regression, the coeficient of determination and the area are listed in Table 2. The table also outlines which lakes are shrinking (left column) or growing (right column) and which are inside or outside the protected area of the State Park. These results are also illustrated graphically in Figure 6.

SHRINKING Inside State Park				GROWING Outside State Park			
Lake	slope	r^2	Area (ha)	Lake	slope	r^2	Area (ha)
141	-0.0039	65.00	31.72	116	0.0032	62.30	63.78
140	-0.0039	78.60	303.24	113	0.0059	57.40	20.26
110	-0.0170	65.90	86.79	111	0.0079	63.30	15.58
109	-0.0058	92.00	68.42	97	0.0120	50.50	224.68
108	-0.0373	68.90	10.27	94	0.0260	74.50	11.86
103	-0.0055	73.00	24.03	87	0.0183	76.20	21.40
45	-0.0093	73.50	24.64	84	0.0070	53.30	20.26
Outside State Park				79	0.0032	70.50	161.77
120	-0.0071	73.10	48.58	28	0.0033	61.30	20.07
118	-0.0068	67.30	31.22	24	0.0049	52.30	64.70
115	-0.0099	61.60	23.93	4	0.0025	51.50	62.85
114	-0.0062	62.50	62.53	2	0.0119	65.60	28.89
85	-0.0347	71.00	15.57				
72	-0.0404	93.60	23.64				
69	-0.0363	60.20	15.75				
55	-0.0350	91.30	21.85				

Table 2. Slope and coefficients of determination for the lakes that have seen their open water area significantly changed during the period of study. The lakes are separated as being inside or outside the Rio Doce State Park. The areas correspond to the vectors interpreted form the 2010 RapidEye image.

2.3 Discussion and future research

The results generated were directly usable to establish an historical progression of the situation of the open water area of over one hundred lakes. The region-based unsupervised classification of the water / non-water classes proved to be fast and accurate when compared with the digitized contours extracted from the Ikonos and RapidEye mosaics. This new approach saved the time and effort that would have been needed to create training samples. Because the study was based on historical data, no validation could be made available. Still, based on the comparison with the visual interpretation, the extraction of the open water area of these lakes proved very accurate, especially when considering their spatial consistency (*i.e.* the contiguousness of the water pixels). Some questions remain open like the density of aquatic plants needed for a pixel to fall in or out of the open water class. It is clear that this parameter depends on the plant species, on the quality of the water and on the time of year (phenology). Because of the large number of similar lakes involved in the study, it stands out that this parameters does not affect the overall results.

However, the results obtained do not agree with our initial hypothesis stating that the degradation of the surroundings of the lakes tend to have a shrinking effect on the open water area of the lakes. Instead, the study shows that the problem is far more complex than we originally expected and that only a thorough and constant monitoring of some of the lakes in various situations could lead to a better understanding. One important observation is that even the lakes in the protected areas are not necessarily safe from the accelerated process of being transformed into bogs or being covered by floating islands. In particular, it has been

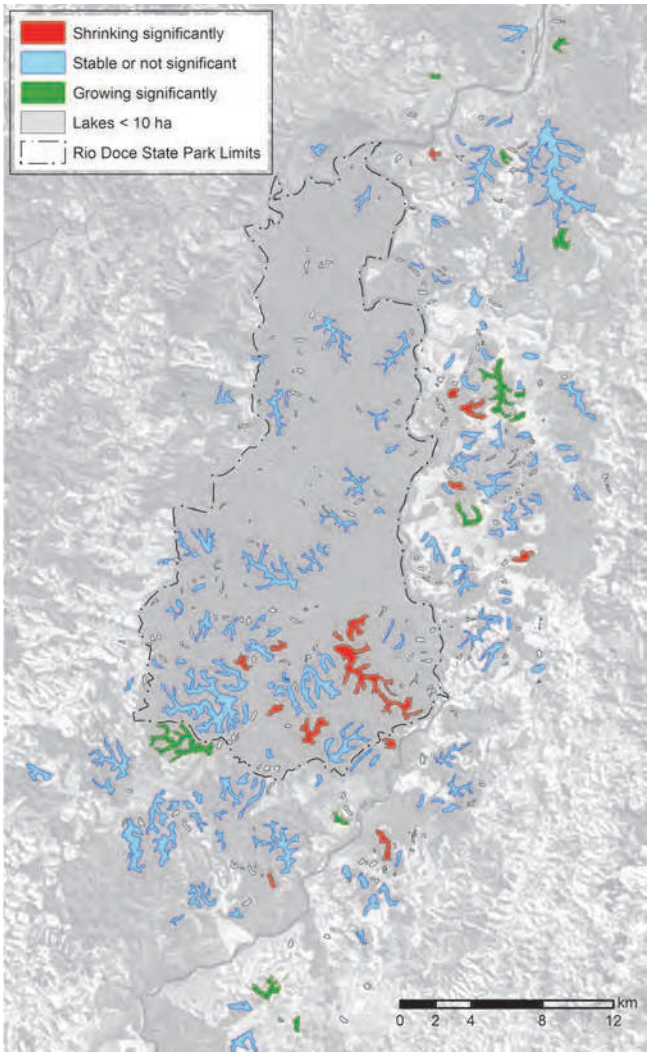

Fig. 6. Image map showing the dynamics of the lakes in the Rio Doce lake system. Only lake larger than 10 ha have been color-coded according to their dynamic state (shrinking or growing). The map overlays band 5 of the 2010 Landsat image (faded).

observed that *Nymphaeaceae caerulea* (a kind of water lily), an exotic plant from Africa, is propagating even in remote lakes, probably through the actions of aquatic birds.

Future research will be focused on acquiring more thorough validation data to classify aquatic communities like it was done in another study of the Pandeiros (Barbosa & Maillard, 2010). It is also planned to implement a program to monitor the dynamic of aquatic plant communities for some lakes that appear to be shrinking or growing both inside and outside the State Park and in different environments (eucalyptus, pasture, forest). Since the Government of Minas

Gerais has implemented a program to acquire RapidEye images of the whole State once or twice a year, this new perspective will facilitate a constant monitoring program with good ground resolution (5 m).

3. Second case study: The receding of six small lakes in the upper Peruaçu watershed

The Cerrado biome as a whole covers over one and a half million square kilometers in Brazil, about 9% of which can be considered semiarid mostly in Northeast Brazil. In Southeastern Brazil the only patch of semiarid Cerrado is at the northernmost tip of Minas Gerais in an ecological tension zone between Cerrado and Caatinga (thorn shrub). The Peruaçu river watershed, a $\approx 1500 km^2$ area falls within this zone and has attracted much attention because of its natural beauty and its archeological and cultural heritage. Receiving less than 1000 mm of precipitations yearly, and having up to seven months without any rain, water resources in the region is critical to the survival of populations but has been suffering from excessive exploitation. In particular, the Veredas do Peruaçu State Park is apparently seeing the continuous lowering of its aquifer in the last few decades. This is mostly observable from the receding of a few small lakes (Figure 7) inside the park and one larger lake outside. Although the phenomenon is obvious to the local population, over exploitation of water resources appears to continue undisturbed.

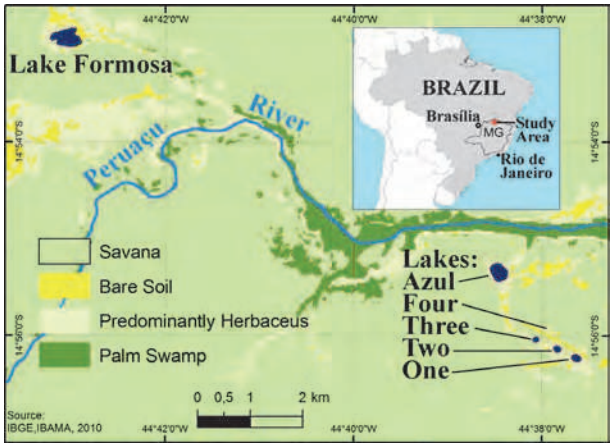

Fig. 7. Location of the six lakes in the Study area near the head waters of the Peruaçu River.

Even though human occupation can be considered sparse, because the Peruaçu watershed is small (1450 km^2) and the region is considered semiarid, we stipulate that the pressure of irrigation, eucalyptus plantations and wells is too great for its supporting capacity. It could be argued that the lowering is caused by local changes in the precipitation and water balance (WB), but since no records of the level of the aquifer or the lakes are available for the past, we had to develop a methodology entirely based on historical remote sensing and meteorological data to unambiguously demonstrate and quantify the phenomenon.

A multi-temporal remote sensing approach was used to create a time sequence of images to monitor the size of the Peruaçu lakes. Landsat images stood as the most logical choice for analyzing the dynamics of these lakes for being the longest record of systematical remote

sensing data available for civil use. Passive optical infrared images are also considered the most effective type of data for delineating water bodies since they absorb almost totally the incoming radiation and produce a sharp contrast with the surrounding vegetation and soil (Bonn & Rochon, 1992; Jensen, 2005).

Considering the small size of the lakes under investigation, the resolution of Landsat TM images is somewhat marginally acceptable because of the mixed pixel problem. The fact that water bodies are smooth continuous surfaces let us postulate that mixed border pixels have a predictable behavior and could be sub-sampled using some interpolation technique.

The objective of this study is to infer the dynamics of the fluctuations of the water level of the aquifer through past monitoring of the successive shrinking and growing of the open water surface of six lakes found in the *Veredas do Peruaçu State Park* and surroundings. To achieve this, we created a methodology for extracting the open water surfaces of these lakes from an historical series of Landsat TM images using interpolation to overcome the mixed pixel problem. We also computed the water balance record for the same period to verify if the behavior of the aquifer can be attributed to modifications in the climate record.

3.1 Material and method

3.1.1 Study area

The study area (Figure 7) is located in Northern Minas Gerais - Brazil, a savannah region that can be marginally classified as semiarid with less than 1000 mm of rain per year. Five of the six lakes under study are inside the limits of the *Veredas do Peruaçu State Park*. The sixth and largest lake Formosa is outside the protected area but still in its immediate vicinities. The hydrographic network is part of the Peruaçu River Basin being a left tributary of the *São Francisco* River. Rainfall is unevenly distributed during the year and is mostly concentrated between November and March. The whole region is mostly flat with deep soils composed mostly of sand and less than 15% of clay that have a low capacity of water retention.

The lakes themselves are small with the largest having an average area of around ten hectares. Because there is no general agreement about the names of the four smaller lakes, they were given the genereic names One, Two, Three and Four while the two larger ones are called Formoza and Azul. Although there has been a few hypothesis to explain the genesis of these lakes and their relative alignment, no conclusive results were ever presented. Lake Four had open water until 2000 but has dried up and is now but an intermittently saturated herbaceous round field. Unofficial reports by the local population all outline the gradual decrease of the open water surface of most of these lakes but no actual study was ever undertaken.

Until the 1970s the region was occupied by small family groups descended from the Indian tribe *Xacriabá*. In the middle of that decade the Brazilian government offered subsidies and incentives to companies that were willing to invest in eucalyptus plantations for wood supply. This was also the beginning of a much denser occupation of the area by workers and farmers. The impacts of the plantations were reflected in the decrease of biodiversity, both in terms of fauna and flora, and also by an increased pressure on water resources. Eucalypt planting ceased in the early 1990's, then the companies abandoned their activities in the region due to low productivity and a practice that was not well adapted to the natural conditions. The region was recognized as having unique biological characteristics and the Brazilian authorities created a national park (*Cavernas do Peruaçu*) and a state park (*Veredas do Peruaçu*) to protect

the natural beauties and the archeological heritage (rock paintings) of the Peruaçu watershed (Maillard et al., 2009). Although the area is now protected by law, the effect of the previous uses can still be observed and the area surrounding the parks still suffer from human pressure, especially on water.

3.1.2 Data and data pre-processing

A total of 51 images from Landsat-5 TM (World Reference System: orbit/scene 219/70) were chosen. Landsat-5 has been continuously collecting image data since 1984 which constitutes the beginning the period considered by this research and ends in 2009. Two images from Landsat-7 ETM+ were also acquired to complete the dataset for the year 2002 for which the Landsat-5 scenes were too cloudy. The dates of the images (Table 3) correspond ideally to the end of the wet season (first image) and the end of the dry season (second image) but had to be slightly shifted in cases where images were either of low quality (clouds) or unavailable. Three images also had to be excluded because they presented calibration problems.

Year	1^{st} image	2^{nd} image	Year	1^{st} image	2^{nd} image	Year	1^{st} image	2^{nd} image
1984	13/jun	13/oct	1985	31/may	06/oct	1986	15/mar	09/oct
1987	02/mar	12/oct	1988	21/apr	30/oct	1989	Excluded	Excluded
1990	10/mar	20/oct	1991	30/apr	07/oct	1992	18/may	23/sep
1993	18/mar	12/oct	1994	22/apr	12/aug	1995	24/apr	02/oct
1996	26/mar	20/oct	1997	09/feb	07/oct	1998	20/jun	26/oct
1999	19/mar	11/sep	2000	24/apr	15/oct	2001	24/mar	01/oct
2002	20/apr*	13/oct*	2003	20/jul	08/oct	2004	01/apr	24/sep
2005	04/apr	13/oct	2006	20/jun	30/sep	2007	Excluded	03/oct
2008	24/feb	05/oct	2009	14/mar	06/sep	2010	4/may**	

Table 3. List of Landsat images (* indicates Landsat-7, the rest are Landsat-5; ** the 2010 image was only used to validate the lake contour extraction method).

The images were geometrically and radiometrically corrected and an atmospheric effect compensation was also applied. The geometric correction was done in an "image-to-image" approach using a one-meter Ikonos image as basis (which was geometrically adjusted using control points from a geodetic GPS survey). The atmospheric and radiometric correction were applied using an in-house program build for that purpose: *Corat_Landsat*. The program takes as input a worksheet containing 1) the name of the image file, 2) the digital number value for the dark object substraction (Chavez Jr., 1988) for bands 1, 2, 3, 4, 5 and 7, 3) the sun elevation angle and 4) the sun-earth distance in astronomical units. The output is a 16 bit reflectance image (reflectance values were redistributed between 0 and 10000).

The calculation of the water balance was based on the method proposed by Thornthwaite & Mather (1955) which consists in determining the hydraulic characteristics of a given region without direct measurements on the ground. The water balance is the simple budget between input and output of water within a watershed:

$$\Delta S = \left(\underbrace{P + G_{in}}_{Inflow} \right) - \left(\underbrace{Q + ET + G_{out}}_{Outflow} \right) \quad (5)$$

where P is the precipitation, G_{in} and G_{out} represents the ground water flow, Q is the runoff water and ET is the evapotranspiration.

The procedure simplifies the calculation by estimating all its components from only two input parameters: average daily temperature and precipitation:

$$AW_t = AW_{t-1} exp\left(-\frac{PET_t}{AWC}\right) \tag{6}$$

where AW_t is the available water at time t, AW_{t-1} is the available water at time $t-1$, PET_t is the potential evapotranspiration at time t and AWC is the soil's water holding capacity. The water balance can be summarized in three situations.

- $\Delta P < 0$; net precipitation (precipitation - potential evapotranspiration) is less than zero: the soil is drying.
- $\Delta P > 0$ but $\Delta P + AW_{t-1} \leq AWC$; net precipitation is more than zero but net precipitation plus the available water from time $t-1$ is less or equal than the soil's water holding capacity: soil is wetting.
- $\Delta P > 0$ but $\Delta P + AW_{t-1} > AWC$; net precipitation is more than zero and net precipitation plus the available water from time $t-1$ is more than the soil's water holding capacity: soil is wetting above capacity and water goes to runoff.

3.1.3 Interpolation and lake contours extraction

Because the lakes are all very small, the 30 m spatial resolution of Landsat TM images became restrictive in terms of contour definition of the lakes. To overcome this limitation, we decided to exploit the very stable behavior of water in the optical infrared region of the electromagnetic spectrum that simply absorbs almost all energy in that part of the spectrum (Ji et al., 2009). In fact, water reflection is almost zero beyond 760 nm (McCoy, 2005). Conversely, the surroundings of all these small lakes is composed of sand and vegetation in large proportion which both reflect much more than water even in the absorbtion bands caused by water content in the leaves as can be seen in Figure 8. In many cases, a simple threshold in an infrared image histogram can reliably separate water from the other land covers with a relatively good rate of success and investigators have developed simple techniques for doing so in a systematical manner (Bryant & Rainey, 2002; Jain et al., 2005). Histograms of near infrared images containing a fair amount of open water surfaces are usually bimodal with the first peak directly related to water. Yet, when one looks closer, the water-land limit is often blurred by a varying width occupied by aquatic plants that can fluctuate over various time scales (yearly or seasonally). Using a sequence of historical Landsat images for which we had no validation data, we needed to have a very strict definition of the water-land interface. We defined the lake "water-edge" as the point at which water overwhelmingly dominates the surface and estimated that point to correspond to 70-80%.

Scale (or spatial resolution) can have various effects on image classification accuracy. A finer resolution can usually decrease the proportion of pixels falling on the border of objects (hence less mixed pixels) which can result in less classification confusion. Conversely, a finer resolution will generally increase the spectral variation of objects that can, in turn increase classification confusion (Markham & Townshend, 1981). Fortunately, water (especially clear and deep) is a spectrally smooth surface for which a finer resolution will bring more benefit

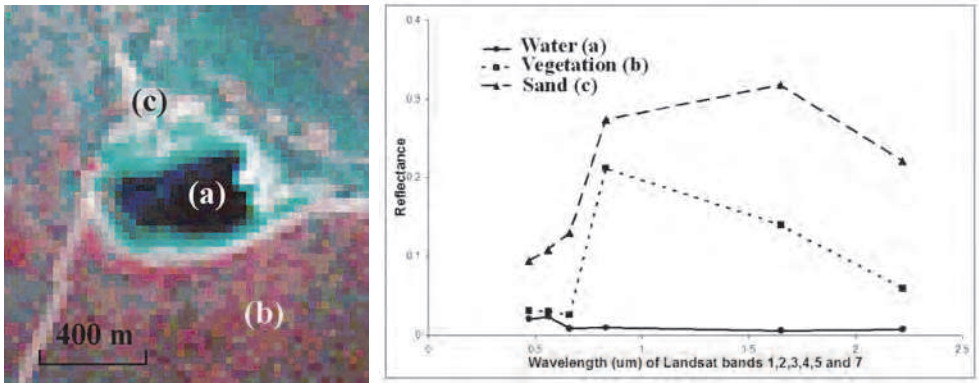

(a) (b)

Fig. 8. Reflectance values samples in a Landsat sub-scene for the visible, near and mid-infrared bands (a) Image section in false color, (b) graph of reflectance values for water, dry savanna vegetation and sandy deposits.

(less border pixels) than disadvantage (spectral variation). This special context led us to stipulate that the lake edge pixels can be subdivided into proportions of water and water edge using a weighted interpolation method. Amongst the various interpolation methods we opted for the minimum curvature interpolation (a variation of bi-cubic spline) with tension as described in Smith & Wessel (1990). This interpolation method has the advantage of being able to generate a smooth surface without generating undesirable fluctuations (artifact peaks or dips) by using a tension parameter. This interpolation proved better than "inverse distance weighted" that tends to produce artifact dips between sampling points (Maune et al., 2001). The minimum curvature worked well and fast and generated smooth ramps while keeping a sharp water-land edge. Figure 9 illustrates the effect of interpolating the Landsat data to 5 m on the lake extraction processing.

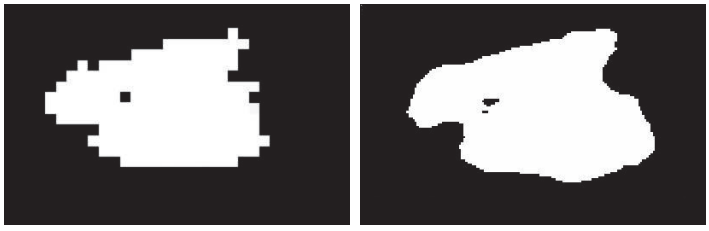

(a) 30 m (b) 5 m

Fig. 9. Comparison of the lake extraction methods using the original 30 m Landsat data (a) and the 5 m interpolated data (b).

3.1.4 Classification

Because the classification was binary in nature (water *vs* non-water), a supervised pixel-based approach was chosen to yield maximum control. Classification approaches such as maximum

likelihood can produce posterior probability maps to which can be applied a threshold (hardened). This approach has the advantage to require training data only for the object of interest whereas classical classification procedures require all classes to have been defined using training data. In this case the posterior probability is simply the Gaussian probability density of the "water" class. In simple nominal classification, a pixel can be classified as pertaining to a particular class even if its probability is low, as long as it is higher than for all the other classes. By using a high threshold value (i.e. $> 90\%$) to attribute a water label to a pixel, we are able to use but a single class and avoid having to gather training data for other objects or surfaces.

3.1.5 Validation

Two validation data sets were used for testing the performance of the extraction of the lake contours from the interpolated Landsat data which also involved our definition of the "water-land" edge. First, the contours from the dry season image of 2006 were compared against the contours extracted from a pan-sharpened Ikonos image (1 m) five days apart from the Landsat image. Secondly, the four lakes of the VPSP (data from the larger lake outside the park could not be acquired) were surveyed using a geodetic GPS in kinetic mode to be compared with the contour from the Landsat image (with a five days difference). Coordinates of the lake contour were acquired at an interval of 15 meters with an approximate precision of 10 cm.

The validation was done by two complementary methods: 1) by expressing the difference between the areas as a proportion of the validated area ($1 - \frac{A_{real} - A_{observed}}{A_{real}} \times 100$); and 2) by overlapping the two contours (interpolated Landsat and validation data) and dividing the overlap area (intersection) by the merged areas (union) of both contours as illustrated in Figure 10. The latter accounts for errors of registration and edge definition of the lakes.

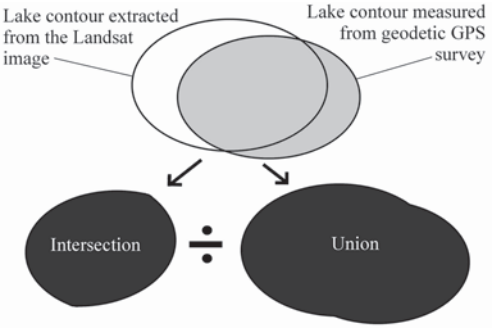

Fig. 10. Validation method for testing the accuracy of the lake contours extracted from the interpolated Landsat images.

3.1.6 Correlation between the lake areas and the water balance

If the behavior of the area of the lakes can be related to a local climate change, then the water budget should be the best indicator of such relationship. Even though the response of the water level to a change in the water budget is not spontaneous, the trend should still be statistically perceptible. Because the areas of the lakes are not normally distributed,

a regression was not recommended. Spearman's correlation does not assume a normal distribution of the dependant variable and was chosen instead. The correlation was also computed between the area of the lakes themselves as a means to infer a generalized trend.

3.2 Results

Figure 11 shows the annual budget averaged every five years for the period along with the average budget for the whole period (black line). Apart from the two first periods (1984-1989 and 1990-1994) which appear as exceptionally high and exceptionally low respectively, the other periods do not show any trend towards an increase or a decrease.

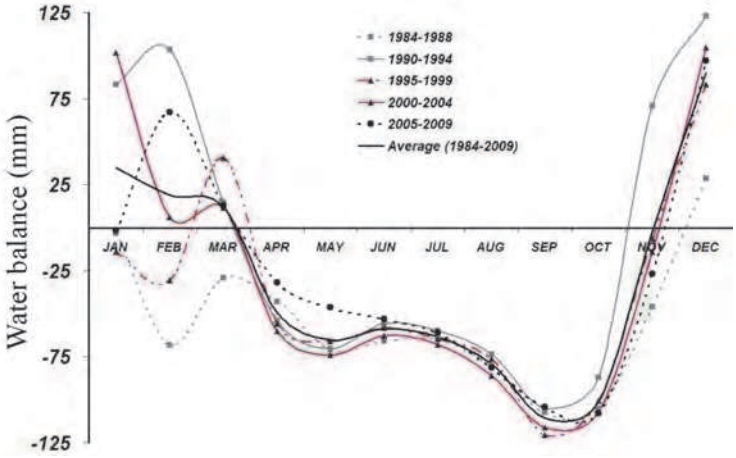

Fig. 11. Water balance over the region averaged for every five years between 1984 and 2009 and overall average (black continuous line).

3.2.1 Extraction and validation of the lake contours

All 51 selected Landsat images were geometrically rectified, registered to a UTM grid, corrected for atmospheric interferences (using Chavez's DOS method) and transformed in reflectance values. The images were then interpolated to a 5 m resolution using a minimum curvature algorithm. Apart from a few exceptions, the multi-temporal dataset shows an almost constant shrinking of the lake surfaces areas and the disappearance of one small water body (Lake Four). Figure 12 shows the 1984 and 2009 image sections side by side to illustrate the shrinking of all six lakes. The triangular area at the bottom of the 1984 image, was part of a eucalyptus plantation and is now naturally regenerating into *cerrado* vegetation.

Extraction of the lake surface area of open water using the posterior probability of the maximum likelihood classification yielded good visual results in all images. This was evaluated by looking at the spatial consistency of the results. Validation of the 2010 classification results confirmed the appropriateness of the methodology. By using the posterior probability of a single water class, we found that there was always an easily identifiable break between the water and non-water classes that made the selection of a threshold very easy. The threshold was applied to all 51 images and the area of all six

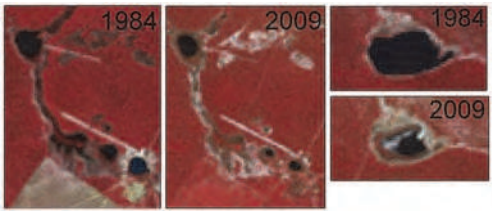

Fig. 12. Comparison of the lakes between October 1984 and September 2009.

lakes computed for every date. The graph in Figure 13 shows how these areas have changes between 1984 and 2009. Table 4 gives an over view of the shrinking of the six lakes. The lake areas of 1990 are also indicated (in bold) for being the record size for all lakes. While Lake Four has completely disappeared since 2000, four other lakes have lost between 59 and 80% of their area. Lake Azul has somewhat retained much more of its original area (loss of 29%) and it is also the only lake surrounded by hydromorphic gley soil with a higher clay content.

Areas	Lakes					
m^2	Four	Three	Two	One	Azul	Formosa
1990	**4962**	**28778**	**37413**	**56402**	**105389**	**296237**
1984	375	14795	32471	39030	92670	291502
2009	0	2928	7228	12243	65829	170409
% loss	100%	80,2%	77,7%	68,6%	29,0%	58,5%

Table 4. Comparison of the areas of all six lakes between 1984 and 2009 with the shrinking expressed in percentage (1990 was the record year for all lakes).

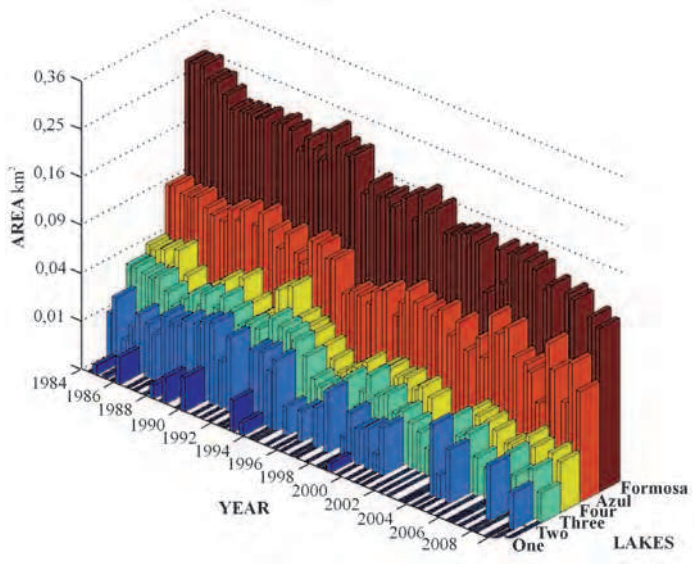

Fig. 13. Graph showing the evolution of the area of all six lakes for the period 1984-2009.

Lakes	Area Comparison		Intersection/Union×100	
	GPS	Ikonos	GPS	Ikonos
Three	94,54%	n/a	81.05%	n/a
Two	93,34%	86,01%	91,53%	71,04%
One	89,50%	94,41%	89,16%	83,85%
Azul	94,18%	96,36%	92,13%	93,20%
Formosa	n/a	95,08%	n/a	92.66%

Table 5. Validation of the lake contour extraction using the GPS survey and the Ikonos scene. Column 2 and 3 show the results for the area comparison; column 4 and 5 show the accuracy obtained with the $\frac{intersection}{union} \times 100$ approach.

Since we did not have precise elevation data, the water surfaces areas could not be associated with precise altimetric level measurements. We used the digital elevation surface (DES) from the ASTER sensor (ground resolution of 30 m) to overlay the contours of the lakes to estimate the height of the water level for the 1984-2009 period. Our analysis shows that Lake Azul has lowered by about 1 meter whereas lakes One, Two, Three and Formosa appear to have lowered by slightly more than 2 meters. Figure 14 shows the 1984 and 2009 levels on the ASTER DES profile for Lake Formosa (we did not, however have access to bathymetric data and the depth of the lake is unknown).

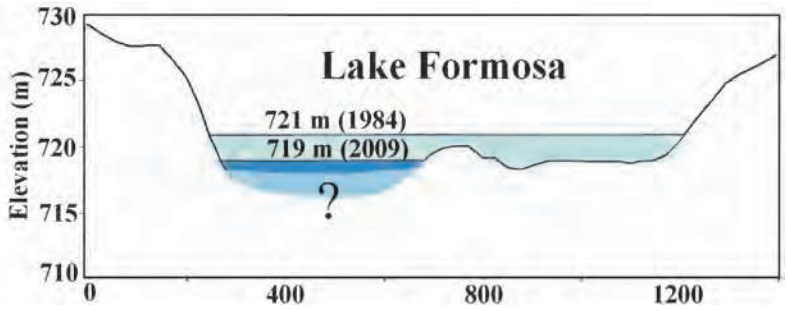

Fig. 14. Water level of Lake Formosa in 1984 and 2009 on an ASTER DES profile.

The validation of the data was done using the approach described in section 3.1.5. Table 5 shows the validation obtained with both control datasets (GPS and Ikonos image) and with the two methods of comparison (simple comparison of areas and "intersection ÷ union" approach). As expected, the accuracies with the latter method are slightly lower but since all accuracies but one are well above 80%, we conclude that both our extraction method and our geometric correction are within very acceptable boundaries. Figure 15 shows the contours extracted from the Landsat image of 2010 and the GPS survey contours for three of the lakes.

3.2.2 Statistical testing

Spearman's correlation test was applied to the area series of all lakes along with the AW data for the same period. The results are presented in Table 6. The only correlation between the areas of the lakes and the AW is Lake Four which has dried up since 2000 and the level of significance is p=0.05. Conversely, all the lakes are strongly related among themselves with a significance of 0.01. This confirms that the trend is statistically significant and that we can

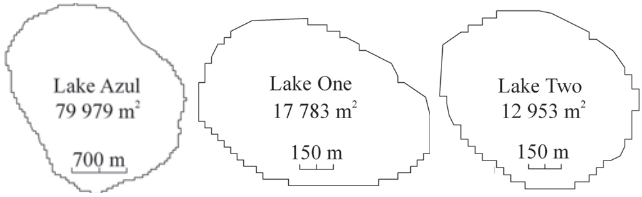

(a) Landsat lake contours (2010)

(b) Geodetic GPS lake contours

Fig. 15. Comparison of the contours of three of the six lakes using the interpolated Landsat data (top) and the geodetic GPS survey data (bottom) made five days after image acquisition.

infer that the lakes are rapidly shrinking. Even Lake Azul which has kept a much more constant surface area is strongly correlated with all the other lakes (0.601 to 0.871). Since the AW cannot be said to be correlated with the shrinking of the lakes, the meteorological explanation becomes much less plausible and the human pressure on the watershed can more easily be pinpointed as responsible.

	AW	**Lakes**				
Lakes		Four	Three	Two	One	Azul
Four	*0.329					
Three	0.209	**0.455				
Two	0.209	**0.611	**0.834			
One	0.075	**0.566	**0.735	**0.957		
Azul	0.259	**0.601	**0.871	**0.866	**0.789	
Formosa	0.068	**0.524	**0.674	**0.899	**0.897	**0.730

* Significant at 0.05 ** Significant at 0.01

Table 6. Results of the Spearman's correlation tests.

3.2.3 Discussion and future research

In this study we proposed an innovative approach for monitoring small lakes using medium resolution Landsat data. The approach uses minimum curvature interpolation to artificially improve the resolution of the image data and produce a much cleaner lake contour that matches the actual measured contour with a high success rate (15 validation out of 16 with better than 80% and 10 better than 90%). Using posterior probability of a maximum likelihood classifier, we were able to systematically extract contours from six lakes for 50 different dates with ease and good matching of control data. Even though we did not have bathymetric data or even precise elevation data of the surroundings of the lakes, the digital

elevation surface produced from ASTER data with a resolution of 30 m, made it possible to estimate that the aquifer lowered, during the 25 year period (1984-2009), by up to two meters. The water balance using the Thornthwaite approach is well suited for area with limited climatological information and provides valuable insight on the climatological condition ruling water availability. In the present case, the water balance could not be statistically correlated (Spearman's correlation) to the shrinking of six small lakes in Northern Minas Gerais, Brazil. It became clear that, if the present situation continues, these small lakes (and the nearby palm swamps) will disappear with drastic consequences for the populations of humans and animals.

Future studies will concentrate on matching the lake size with precise elevation data and piezometric measurements. Although Landsat data proved most useful for extracting the open water surface, we plan to shift towards more precise satellite data such as RapidEye for which the Minas Gerais Government is acquiring on a regular base (twice a year) for the whole state. Future research will also explore more thoroughly the possibilities of artificially increasing resolution through interpolation. More interpolations methods need to be tested and compared with various situations. With the recent installation of a nearby weather station, precise local data will yield better control on monitoring the water budget throughout the year.

4. Overall conclusions

Multi-temporal remote sensing offers countless opportunities for monitoring past and present changes in land cover and land use. By monitoring the size and shape of water bodies, we can infer on human pressure and climate change. Small water bodies are especially fragile areas with a very high ecological value (the value of the services provided by lakes and wetlands has been considered as high as 8.498 and 14.785 $\$ha^{-1}yr^{-1}$ respectively according to Costanza et al., 1997) that are very sensitive to changes in temperature or the equilibrium of nutrients input (Mitsch & Gosselink, 2000).

In this chapter, two new approaches for monitoring small lakes and wetlands were used. First by using a region-based unsupervised classification based on an hybrid implementation (watershed and Markov random fields) we ensured a non-arbitrary systematic approach that did not rely on training samples or a subjective threshold. The MAGIC program proved very reliable for processing a large number of scenes while maintaining a very stable and predictable behavior. Although it turned out to work better by choosing a larger number of classes than actually needed, finding the water class was always easy and could easily be automated in certain cases like this one (for example by ordering the signatures through their mean). Future work will concentrate on determining the parameters that govern the precise amount of water within a pixel for it to fall in the water class.

Secondly, an interpolation method was used to artificially increase the resolution (from 30 m to 5 m) of a series of Landsat images to improve the contour definition of a set of very small lakes and to characterize their dynamic throughout a 25 years period. Much care was taken to validate the methodology by using two distinct methods of validation to account for all type of errors. The validation yielded a precision between 80% and 93% in all cases except one. Future work will concentrate on having this approach improve by using precise elevation data to associate an actual water level with the size of the lakes.

The use of historical satellite data is often made difficult by the absence of validation data and one must generally rely of sparse observations to corroborate results. One solution lies

on validating the methodology using recent data and then to apply it to the historical data. Landsat has been an invaluable source of data since the 80's (Thematic Mapper) and even the 70's (Multi Spectral Scanner) by systematically acquiring data at regular predictable intervals over the same region. The newer generations of satellites platforms work mostly on a "per demand" scheme and require more carefully planned logistics of image acquisition. It is also likely that future post-Landsat multi-temporal studies will have to deal with data from different sensors with different resolutions and even different spectral specifications. This will bring new challenges to multi-temporal studies for which much research is still needed.

5. Acknowledgements

The authors are thankful to the Forestry Institute of Minas Gerais (IEF-MG) for providing the Ikonos and RapidEye data and field support. We are most thankful to Thaís Amaral Moreira for her hard work in mapping and statistics.

6. References

Barbosa, I. & Maillard, P. (2010). Mapping a wetland complex in the Brazilian savannah using an Ikonos image: assessing the potential of a new region-based classifier, *Canadian Journal of Remote Sensing* 36(Suppl. 1): S231–S242.

Bonn, F. & Rochon, G. (1992). *Précis de Télédétection: Principes et Méthodes*, Vol. 1, Presses de lt'Université du Québec. 485 p.

Bryant, R. G. & Rainey, M. (2002). Investigation of flood inundation on playas within the zone of chotts, using a time-series of AVHRR, *Remote Sensing of Environment* (3): 360–375,.

Chavez Jr., P. S. (1988). An improved dark-object subtraction technique for atmospheric scattering correction of multispetral data, *Remote Sensing of Environment* 24(2): 459–479.

Clausi, D. A., Qin, K., Chowdhury, M. S., Yu, P. & Maillard, P. (2010). Magic: Map-guided ice classification, *Canadian Journal of Remote Sensing* 36(Suppl. 1): S13–S25.

Costanza, R., d'Arge, R., de Groot, R., Farber, S., Grasso, M., Hannon, B., Limburg, K., Naeem, S., O'Neill, R. V., Partuelo, J., Raskin, R. G., Sutton, P. & van den Belt, M. (1997). The value of the world's ecosystems services and natural capital, *Nature* 387(15 May): 253–260.

Deng, H. & Clausi, D. A. (2005). Unsupervised segmentation of synthetic aperture radar sea ice imagery using a novel Markov random field models, *IEEE Trans. on Geoscience and Remote Sensing* 43(3): 528–538.

Esteves, F. A. (1988). *Fundamentos de limnologia*, 2nd edn, Interciência, Rio de Janeiro.

Geman, D., Geman, S., Graffigne, C. & Dong, P. (1990). Boundary detection by constrained optimization, *IEEE Trans. Pattern Anal. Machine Intell.* 12(7): 609–628.

Gilhuis, J. P. (1986). *Vegetation survey of the Parque Florestal Estadual do Rio Doce, MG, Brasil*, Master's thesis, Universidade Federal de Viçosa, Brazil.

Ikusuma, I. & Gentil, J. G. (1985). *Limnological Studies in Central Brazil, Rio Doce Valley Lakes and Pantanal Wetland (1st Report)*, Water Reseach Institute, Nagoya University, chapter Macrophyte and its environment in four lakes in Rio Doce Valley.

Jain, S. K., Singh, R. D., Jain, M. K. & Lohani, A. K. (2005). Delineation of flood-prone areas using remote sensing technique, *Water Resources Management* 19(4): 337–347.

Jensen, J. R. (2005). *Introductory Digital Image Processing*, 3rd edn, Pearson Prentice Hall, New Jersey. 526 p.

Ji, L., Zhang, L. & Wylie, B. (2009). Analysis of dynamic thresholds for the normalized difference water index, *Photogrammetric Engineering and Remote Sensing* 75(11): 1307–1317.

Junk, W. J. & Silva, C. J. (1999). O conceito do pulso de inundação e suas implicações para o pantanal de Mato Grosso, *Anais do II Simpósio sobre Recursos Naturais e Sócio-Econômicos do Pantanal*, EMBRAPA-DDT, pp. 17–28.

Li, S. Z. (1995). *Markov Random Field Modeling in Computer Vision*, Springer-Verlag, New York, NY, USA.

Maillard, P., Alencar-Silva, T. & Clausi, D. A. (2008). An evaluation of radarsat-1 and aster data for mapping *veredas* (palm swamps), *Sensors (MDPI)* 8: 6055–6076.

Maillard, P., Augustin, C. H. R. R. & Fernandes, G. W. (2009). *Arid Environments and Wind Erosion*, Novascience Publisher, chapter Brazil's Semiarid Cerrado: A Remote Sensing Perspective.

Markham, B. L. & Townshend, J. R. G. (1981). Land cover calssification accuracy as a function of sensor spatial resolution, *Proceedings of the 15th Int. Symp. on Remote Sensing of the Environment*, Ann Arbor, MI, pp. 1075–1090.

Maune, D. F., Kopp, S. M., A., C., Crawford & Zerdas, C. E. (2001). *Digital Elevation Model Technologies and Applications*, 1 edn, American Society for Photogrammetry and Remote Sensing, Bethesda, MD, chapter Introduction, pp. 1–34.

McCoy, R. (2005). *Field Methods in Remote Sensing*, The Guildford Press, 159 p., New York, NY.

Meis(de), M. R. M. & Tundisi, J. (1986). Geomorphological and limnological processes as a basis for lake typology: the middle Rio Doce lake system, *Anais da Academia Brasileira de Ciências* 58(1): 103–120.

Mitsch, W. & Gosselink, J. (2000). *Wetlands*, John Wiley and Sons, New York, NY, USA.

Pivari, M. O. D., Pott, V. J. & Pott, A. (2008). Macrófitas aquáticas de ilhas flutuantes (baceiros) nas sub-regiões do Abobral e Miranda, Pantanal, MS, Brasil, *Acta Botanica Brasilica* 22(2): 559–567.

Pott, V. J. & Pott, A. (2003). *Ecologia e manejo de macrófitas aquáticas*, Editora da Universidade Estadual de Maringá, chapter Dinâmica da vegetação aquática do Pantanal, pp. 145–162.

Smith, W. H. F. & Wessel, P. (1990). Gridding with a continuous curvature surface in tension, *Geophysics* 55: 293–305.

Thornthwaite, C. W. & Mather, J. R. (1955). *The water balance*, Publications in Climatology, Drexel Institute of Technology, New Jersey.

Tso, B. & Mather, P. (2001). *Classification Methods for Remotely Sensed Data*, Taylor and Francis, London, England.

Tundisi, J. G., Matsumura-Tundisi, T., Pontes, M. & Gentil, J. (1981). Limnological studies at quaternary lakes in eastern Brazil, *Revista Brasileira de Botânica* 4: 5–14.

Veloso, H. P., Rangel Filho, A. R. L. & Lima, J. C. A. (1991). *Classificação da Vegetação Brasileira Adaptada a um Sistema Universal*, Rio de Janeiro: FIBGE.

Vincent, L. & Soille, P. (1991). Watersheds in digital spaces: an efficient algorithm based on immersion simulations, *IEEE Transactions on Pattern Analysis and Machine Intelligence* 13(6): 583Ű598.

Xu, H. (2006). Modification of normalised difference water index (NDWI) to enhance open water features in remotely sensed imagery, *International Journal of Remote Sensing* 27(14).

Yu, Q. & Clausi, D. A. (2008). IRGS: image segmentation using edge penalties and region growing, *IEEE Trans. Pattern Analysis and Machine Intelligence* p. paper accepted for publication.

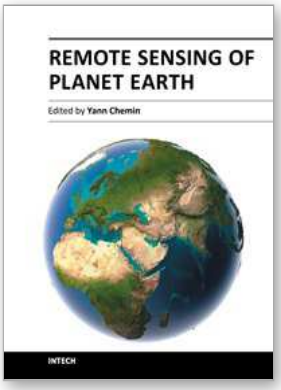

Remote Sensing of Planet Earth

Edited by Dr Yann Chemin

ISBN 978-953-307-919-6
Hard cover, 240 pages
Publisher InTech
Published online 27, January, 2012
Published in print edition January, 2012

Monitoring of water and land objects enters a revolutionary age with the rise of ubiquitous remote sensing and public access. Earth monitoring satellites permit detailed, descriptive, quantitative, holistic, standardized, global evaluation of the state of the Earth skin in a manner that our actual Earthen civilization has never been able to before. The water monitoring topics covered in this book include the remote sensing of open water bodies, wetlands and small lakes, snow depth and underwater seagrass, along with a variety of remote sensing techniques, platforms, and sensors. The Earth monitoring topics include geomorphology, land cover in arid climate, and disaster assessment after a tsunami. Finally, advanced topics of remote sensing covers atmosphere analysis with GNSS signals, earthquake visual monitoring, and fundamental analyses of laser reflectometry in the atmosphere medium.

INTECH
open science | open minds

InTech Europe
University Campus STeP Ri
Slavka Krautzeka 83/A
51000 Rijeka, Croatia
Phone: +385 (51) 770 447
Fax: +385 (51) 686 166
www.intechopen.com

InTech China
Unit 405, Office Block, Hotel Equatorial Shanghai
No.65, Yan An Road (West), Shanghai, 200040, China
中国上海市延安西路65号上海国际贵都大饭店办公楼405单元
Phone: +86-21-62489820
Fax: +86-21-62489821